

NUMERICAL SIMULATION OF SHALLOW TUNNELS LINED IN STEEL REINFORCED CONCRETE CONSIDERING THE EFFECTS OF CRACKING

Betina M. Jensen

Denise Bernaud

Américo Campos Filho

betina.jensen95@gmail.com

denise.bernaud@ufrgs.br

americo@ufrgs.br

*Department of Civil Engineering, Federal University of Rio Grande do Sul - UFRGS
99 Osvaldo Aranha Ave, 90035-190, Porto Alegre - Rio Grande do Sul, Brazil*

Abstract. Tunnel design requires the correct evaluation of both soil strains and lining stresses levels through an analysis that must contemplate the soil-structure interaction and the excavation process. When tunnels are installed close to the ground surface, the complexity of the problem increases in comparison to deep tunnels, since shallow tunnels show an ovalized shape of the deformed cross-section and a heterogeneous stress field around the excavation, inducing tension stresses to appear and possibly resulting in the cracking of the concrete lining. In this context, this paper presents a numerical simulation in finite elements, with the software Ansys, focused on the study of the structural behavior of shallow tunnels lined in steel reinforced concrete. To perform such analysis, the soil mass was represented by a plastic model using the Mohr-Coulomb criterion and, regarding the concrete, three different models of behavior were admitted: an elastic, a viscoelastic and a viscoelastic with cracking consideration. Moreover, the embedded reinforcement model was adopted to represent the steel reinforcement of the concrete. The results obtained in the investigation indicate the influence of the cracking consideration in the tunnel model, which modifies the stresses field of the lining and causes higher values of final convergence.

Keywords: Shallow tunnels, Finite element method, Concrete, Cracking.

1 Introduction

The stress and strain levels of a tunnel lining depend on several factors, such as the interaction of this lining with the soil mass where the tunnel will be excavated and the respective characteristics of these materials, in addition to the excavation method employed. The strains resulting from the excavation reduce the existing pressures in the soil mass and induce stresses in the lining that correspond to a portion of this initial geostatic pressure (ITA [1]; El Nahhas et al. [2]).

Dealing with shallow tunnels, that are located at a small depth compared with the size of their cross-section, the complexity of the problem increases, since this type of tunnel is influenced by the free ground surface above it and presents an ovalized cross-sectional deformed shape, different of the uniform deformed shape usually seen in deep tunnels (Pinto & Whittle [3]). Besides that, since shallow tunnel lining is subjected to lower compression levels than those situated at higher depths, it is important to consider the coefficient of earth pressure at rest (K), which modifies the value of the horizontal pressures in relation to the vertical ones, as different from the unit (characteristic of common soils). On the other hand, treating the horizontal pressure acting on the ground as equal to the vertical pressure (simplification often used in deep tunnels analysis) may have a significant impact on the results, as the K coefficient makes some cross-sectional regions less compressed than others. Thus, since the tunnel lining is subject to bending-compressive stresses, a shallow tunnel becomes more susceptible to the emergence of tensile stresses and consequent cracking of the concrete, which may reduce its stiffness and induce higher strains.

This paper, originated from the master thesis of the first author (Jensen [4]), presents a finite element model elaborated with Ansys software, which performs the tunnel excavation and lining placement processes with the tool of activation and deactivation of elements, step by step. In order to represent the behavior of the soil mass where the tunnel is excavated, the Mohr-Coulomb plasticity criterion was chosen. The behavior of the concrete was represented by three different models: linear elastic, viscoelastic and viscoelastic considering the effects of cracking. Since these two last-mentioned models are not previously available in the software chosen, Ansys's User Programmable Features (UPF) tool is used, based on the studies of Quevedo [5] and Schmitz [6]. Besides, the steel reinforcement is represented by an embedded reinforcement model.

The purpose of the analysis performed was, thereby, to determine the difference between the consideration of concrete behavior through the three models mentioned, along with a variation also in the depth of the analyzed tunnel. Furthermore, by fixing depth and the concrete behavior as viscoelastic with cracking, the influence of other parameters involved was also studied.

2 Mechanical behavior of tunnels

In the study of mechanical and structural behavior of a tunnel, it is very important to consider in the analysis the constructive phases, related to the excavation of the soil mass. During excavation, the region near to the tunnel advancing cross-section (called excavation face) is subjected to higher stresses and strains gradients; hence, it can be stated that this part of the tunnel consists in an influence zone that starts from a cross-section located inside the not excavated soil mass, where the radial displacements are small, to another section located in the excavated part, where the displacements reach maximum values (Lunardi [7]; Gomes [8]; Couto [9]).

The radial displacements define the so-called tunnel convergence, a parameter defined by the relation between these displacements in a given section and the tunnel radius. Figure 1 shows the convergence of a circular tunnel in relation to the excavation sections: null in a region of the unexcavated soil mass far from the excavation front, with a maximum gradient in the region around the excavation front and maximum value in an excavated region far from the front.

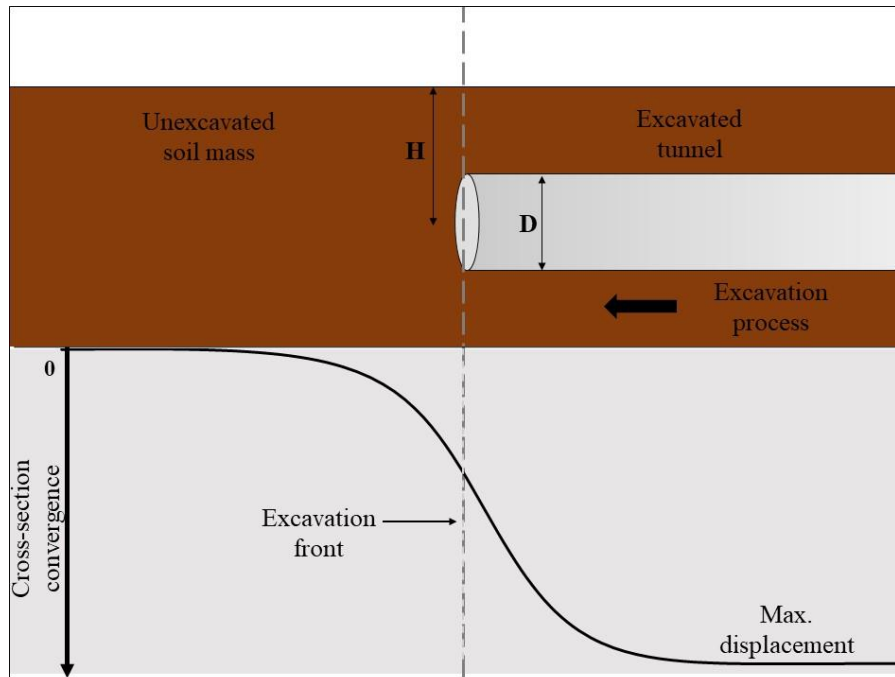


Figure 1 – Tunnel convergence along the longitudinal section to the excavated and unexcavated parts.

Numerical methods are an important tool to determine soil mass displacements and project the tunnel lining, since they present several advantages over analytical and empirical methods. Besides allowing the adoption of nonlinear and distinct constitutive models for the soil and the lining, the modeling of complex geometries and the consideration of boundary and loading conditions similar to those found in the field, the numerical simulations enable to reproduce the excavation process and the placement of the lining by the elements activation and deactivation method. In this method, the excavation and lining placement sequences are simulated by changing the stiffness value of the affected elements at each excavation step. To represent the removal of the soil mass, the stiffness of the excavated elements is reduced while, in order to simulate the support placement, the mechanical characteristics of the respective elements, which were previously related to the soil, are changed for concrete.

2.1 Shallow tunnels

The distribution of stresses in the soil mass, the order of magnitude of the displacements on the ground surface and the degree of displacements symmetry above and below the cross-section of the tunnel are some aspects that distinguish the tunnels between shallow and deep. In practice, it is possible to differentiate these two types of tunnel through the relationship between their depth and diameter (H/D) and, although there is no accordance about the limit value, the adoption of the relation $H/D < 10$ (adopted, for example, in the studies by Benamar [10] and Ferrão [11]) seems appropriate.

The stresses field developed around a shallow tunnel is not purely radial like in deep tunnels, due to the influence of the proximity with the free ground surface. Consequently, the cross-sectional deformation of a shallow tunnel is not merely uniform and related to the volume change of the cavity. In fact, in accordance with Pinto and Whittle [3], two other components that form the final deformed state appear: distortion (or ovalization) and vertical translation. The difference in the deformed shape from shallow to deep tunnels is shown in Fig. 2.

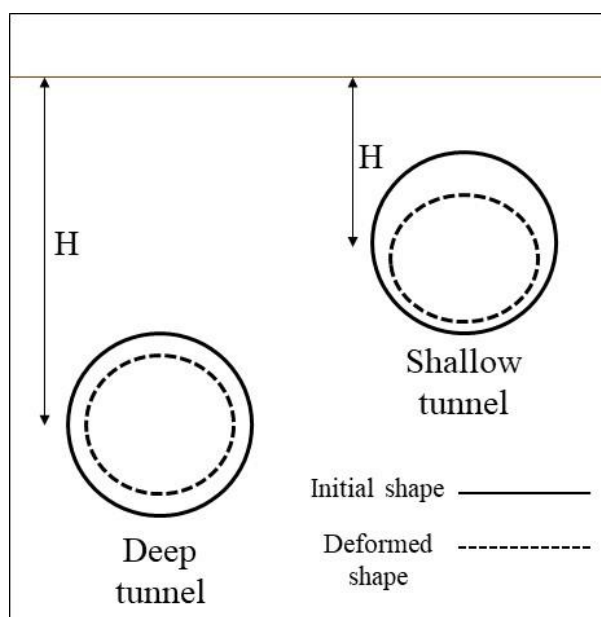


Figure 2 - Difference in the shape of deep and shallow tunnels deformed cross-section.

Furthermore, once located at lower depths (closer to the ground surface), for shallow tunnels it should be considered as acting in the soil mass different pressures than the geostatic-hydrostatic ones. The coefficient of earth pressure at rest (K), for example, which modifies the value of the horizontal pressures in relation to the vertical ones, must be taken into account, as the soil weight is relatively small at lower depths and, as a consequence, the compression level at which the lining is subjected is lower, possibly making the anisotropy induced by K to cause the appearance of tensile stresses.

2.2 Tunnel lining

The tunnel lining is the structural system installed with the purpose of provide the necessary support to the tunnel, assisting the soil mass in the stabilization of strains during the construction and use stages of the structure, as well as other functions such as limiting water infiltration and serving as the basis for the final inner tunnel surface. In general, this is a hyperstatic problem, since the stresses acting in the lining, the stresses resulting from these solicitations and the displacements caused are interdependent and related to the joint soil mass-support behavior.

The stresses developed in the tunnel lining depend on several factors, one of which is the lining stiffness. For a better understanding of stiffness influence, Peck [12] suggests that two main situations should be assumed, both for a circular tunnel with lining. If the tunnel lining was perfectly flexible but able to withstand the radial pressures compressing it, tangential and shear stresses would not appear and therefore there would be no bending moments. On the other hand, assuming this lining to be perfectly rigid, the pressures would cause bending moments due to the lining resistance to the strains that would be imposed. In practice, however, the lining stiffness is intermediate between the two cases proposed. In this way, the tunnel equilibrium cannot be reached only by changing its diameter, and this distortion may induce the appearance of some bending moments.

3 Constitutive models of materials

This item aims to describe the constitutive models adopted in the analysis performed for the materials that compose the tunnels: the soil mass; and the lining, in steel reinforced concrete.

3.1 Soil mass

To represent the behavior of the soil mass, it is employed the constitutive model of Mohr-Coulomb, often adopted as a resistance criterion in the geotechnical engineering. A version of this model is provided by Ansys [13] and could be applied by the insertion of parameters as the friction angle (ϕ), the cohesion (C) and the dilatancy angle (ψ) of the material.

In general, the Mohr-Coulomb criterion considers that the yielding of the material occurs when the shear stress reaches the limit criterion, given in the Eq. (1):

$$\tau = C - \sigma \tan \phi. \quad (1)$$

Then, the cohesion is the shear stress that causes the yielding when the medium stress is null and the friction angle defines the increase in the yielding to the extent that the medium stress increases. For a generalized state of stresses, the Mohr-Coulomb yielding surface can be written by Eq. (2), in terms of the stress invariants:

$$f_{MC}(\sigma) = \sigma_m \sin \phi + \frac{\sigma_e}{\sqrt{3}} \left(\cos \theta - \frac{\sin \theta \sin \phi}{\sqrt{3}} \right) - C \cos \phi. \quad (2)$$

In which:

$$\sigma_e = \sqrt{3J_2} \quad (3)$$

$$\sin 3\theta = -\frac{3\sqrt{3}}{2} \frac{J_3}{\sqrt{J_2^3}}. \quad (4)$$

And the stress invariants are given by Eq. (5), (6) e (7):

$$I_1 = \sigma_{11} + \sigma_{22} + \sigma_{33} \quad (5)$$

$$J_2 = \frac{1}{6} \left[(\sigma_{11} - \sigma_{22})^2 + (\sigma_{22} - \sigma_{33})^2 + (\sigma_{33} - \sigma_{11})^2 \right] + \tau_{xy}^2 + \tau_{yz}^2 + \tau_{xz}^2 \quad (6)$$

$$J_3 = \det(\sigma - I\sigma_m). \quad (7)$$

3.2 Lining

This research aimed to contemplate two behaviors presented by the concrete: the one to present time-dependent strains and the other one to present low resistance to tensile stresses. Thus, to implement a viscoelastic model with consideration of the cracking effects, it was necessary to use the Ansys customization tool, the User Programmable Features - UPF, more precisely the UserMat subroutine, specific to customize material behavior. For this, the studies of Lazzari [14], Quevedo [5], Schmitz [6] and Quevedo et al. [15] were used, in which further details on formulations and solution processes can be found.

The time-dependent behavior of the concrete can be explained in terms of the creep and shrinkage phenomena. The first one concerns the continuous and gradual increase of strains under uniform stresses and can be separated, as in the case of the Solidification Theory proposed by Bazant and Prasannan [16], in a portion dependent on the load age and another part dependent on the concrete age, same distinction made by the formulation given by the *Comité Euro-International du Béton* (CEB-FIP MC90) [17]. The second phenomenon, called shrinkage, refers to the volume reduction of the material given by the gradual water loss remaining in the capillary vessels inside the concrete, if it has not been completely used in the hydration reactions of the cement.

The *Comité Euro-International du Béton* [17] shows the total strain in the age t of a concrete element uniaxially charged in age t_0 with uniform stress $\sigma_c(t_0)$ dealing with the Eq. (8):

$$\varepsilon_c(t) = \varepsilon_{ci}(t_0) + \varepsilon_{cc}(t) + \varepsilon_{cs}(t) + \varepsilon_{ct}(t) = \varepsilon_{c\sigma}(t) + \varepsilon_{cn}(t). \quad (8)$$

In which:

- $\varepsilon_{ci}(t_0)$ = initial elastic and linear strain (immediate);
- $\varepsilon_{cc}(t)$ = creep strain;
- $\varepsilon_{cs}(t)$ = shrinkage strain;
- $\varepsilon_{ct}(t)$ = thermal strain.

Thus, the total strain is composed by a dependent of the stress part ($\varepsilon_{c\sigma}(t)$), where the elastic and the creep strains are included, and other independent of the stress ($\varepsilon_{cn}(t)$), that comprises the shrinkage and the thermal strains, highlighting that the latter is not addressed in this paper.

The strain that depends on the stress can be expressed by the Eq. (9):

$$\varepsilon_{c\sigma}(t, t_0) = \sigma_c(t_0) \left[\frac{1}{E_c(t_0)} + \frac{\phi(t, t_0)}{E_{ci}} \right] = \sigma_c(t_0) J(t, t_0). \quad (9)$$

In Eq. 9, $J(t, t_0)$ is the creep function and refers to the terms given by the Eq. (10):

$$J(t, t_0) = \frac{1}{E_c(t_0)} + \frac{\phi(t, t_0)}{E_{ci}}. \quad (10)$$

The other terms are:

- $\sigma_c(t_0)$ = uniform stress applied in the initial time (MPa);
- $E_c(t_0)$ = concrete tangent elasticity modulus in the initial time (MPa).
- $\phi(t, t_0)$ = creep coefficient;
- E_{ci} = Young modulus at the age of 28 days (MPa).

To the shrinkage strain, the *Comité Euro-International du Béton* [17] defines the relation below (Eq. (11)):

$$\varepsilon_{cs}(t, t_s) = \varepsilon_{cs0} \beta_s(t - t_s). \quad (11)$$

In which:

- t_s = concrete age when shrinkage starts (days);
- ε_{cs0} = shrinkage factor that depends on the concrete age and not on the shrinkage age;
- $\beta_s(t - t_s)$ = factor that depends on the shrinkage age ($t - t_s$).

It is worth noting that, in accordance with Quevedo et al. [15], the use of the *Comité Euro-International du Béton* [17] formulation is due to the fact that the creep model fits into the Bazant and Prasannan Solidification Theory [16], which facilitates the numerical solution of the concrete time-dependent behavior considering aging as an isolated factor (related only to the volume of solidified concrete over time).

In turn, the concrete's ability to withstand less tensile stresses than compressive stresses can result in cracking even at low stress levels (to which shallow tunnels are generally subjected, for example). In order to verify if cracking occurred, the stress level of the integration points is evaluated in two procedures: one that verifies if the integration points stresses reached the yield surface adopted, that in this research was that of Ottosen [18], and another one that evaluates if cracking or crushing failure occurs (the cracking failure occurs if the first principal stress of the sample point is equal or greater than the half of the concrete average tension strength).

The cracking consideration for the points that have reached the mentioned criteria occurs through a model of distributed cracks, in which only material properties are modified, without being necessary to modify the finite element mesh. In this case, as in the studies of Lazzari [14] and Schmitz [6], the crack is considered to be formed in a plane perpendicular to the main stress direction and the longitudinal and transverse elasticity modulus are reduced, in addition to neglecting the Poisson effect.

Dealing with reinforced concrete, even after cracking, the concrete continues to resist certain tensile stresses due to the tension stiffening effect. One of the ways to represent this phenomenon in the model is to modify the stress-strain curve of the concrete, which becomes linear with softening, as shown in Fig. 3. A constitutive relation that describes this behavior, proposed by Martinelli [19], is given by Eq. (12):

$$\sigma_c = 0.6E_{ci}\varepsilon_t \left(1 - \frac{\varepsilon_c}{\varepsilon_{cTU}} \right) = 0.6\sigma_t \left(1 - \frac{\varepsilon_c}{0.001} \right). \quad (12)$$

In which:

σ_c = concrete stress;

E_{ci} = tangent elasticity modulus;

ε_t = tensile nominal strain in the cracked zone;

ε_c = concrete strain;

σ_t = tensile stress in the cracked zone;

ε_{cTU} = limit of tensile strain, which defines the end of the softening portion.

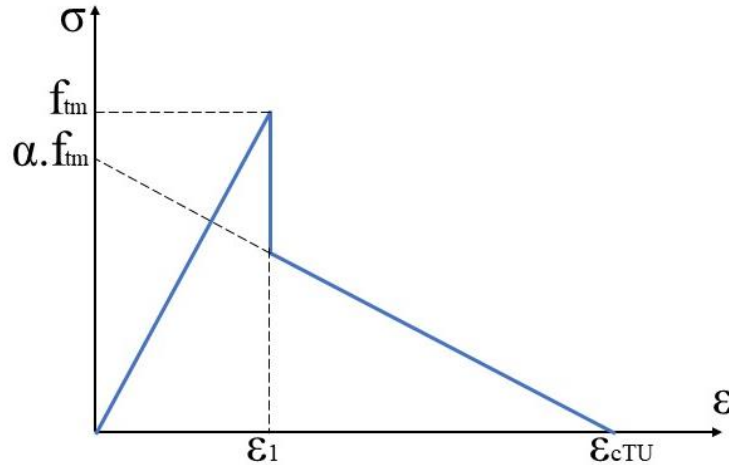


Figure 3 – Stress-strain curve for the tensile concrete.

Besides the consideration of the tension stiffening effect, a gradual reduction of shear stresses in the crack plane is also taken into account, as suggested by Hinton [20]. To represent this phenomenon in an approximate way, the transverse elasticity modulus of the material is multiplied by a reducing factor.

Finally, the steel reinforcement bars of the lining, which resist only axial forces and their behavior can be described by a uniaxial model. Thus, the steel is represented by a bilinear stress-strain diagram and has a perfect elastoplastic behavior, although a small hardening factor is applied to avoid numerical errors, as recommended by Schmitz [6].

4 Numerical analysis

This item presents details about the numerical modeling, describing the finite elements used, the mesh adopted and other characteristics of the model. Next, the results of the simulations performed are shown.

4.1 Ansys numerical modeling

The finite element used in the model to represent both soil and concrete is the SOLID185, which has 8 nodes with 3 d.o.f per node (translation in x, y and z). To represent the steel bars, the element adopted is the REINF264, an incorporated reinforcement element which has only axial stiffness and could be placed in any orientation within the base element.

The numerical simulation of the tunnel construction process is done by 37 excavation steps, which measure, each one, one-third of the external tunnel radius, so that the final model has an excavated part (more discretized) and an unexcavated part, with 15678 finite elements in total. The excavation process, simulated by the elements activation and deactivation tool, is done with the Ansys Birth and

Death commands. First, it is generated a duplicate mesh in the lining region; then, the elements that represent the concrete are soon disabled to, finally, step by step, deactivate the soil mass elements as those of the lining are reactivated.

Figure. 4 shows the (a) 3D mesh and their respective (b) longitudinal and (c) transverse sections, and brings the boundary conditions (restriction to the displacement in Y in the lower face and in Z in the front face) and loads ($P_v = \gamma.H$ and $P_h = K.P_v$, with γ the soil specific weight, H the tunnel height and K the earth pressure coefficient). Furthermore, it is applied a symmetry condition in the ZY plan and, as a consequence, only half of the model is simulated.

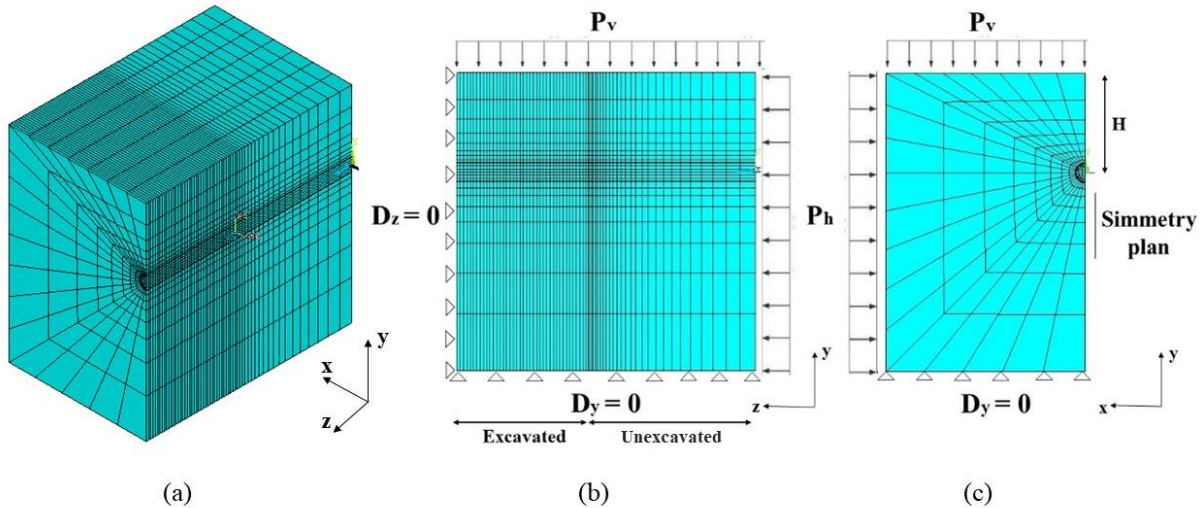


Figure 4 – (a) 3D mesh, (b) longitudinal section and (c) transverse section of the model.

4.2 Results

Some simulations are carried out to compare the results obtained by altering the behavior models of the materials, where it is expected to analyze the influence of to consider or not the cracking of the lining rather than contemplating only an elastic or viscoelastic behavior. The objective is to obtain the displacements in a region far from the excavation face, in three points of the tunnel cross-section: at 90° , 180° and 270° (Fig. 5), for three distinct constitutive models.

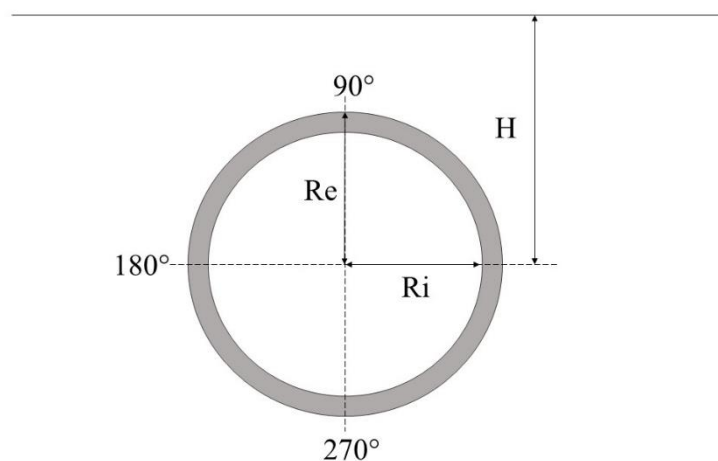


Figure 5 – Points of analysis results in the tunnel cross-section.

For the soil mass, a plastic behavior is admitted by assuming the Mohr-Coulomb criterion, as already explained in item 3.1. As for the lining, it is expected to evaluate the evolution of the tunnel convergence as the model changes between: elastic, viscoelastic and viscoelastic with cracking (all with

steel reinforcement). The tunnel depth will also be varied so that its influence on the results can be analyzed. The necessary parameters for the analysis of a circular tunnel are those shown in Tab. 1.

In order to intensify the solicitations undergone by the lining, which can contribute to the cracking occurrence in the concrete, the distance of the lining placement in relation to the excavation front (or unlined length) (d_0) is considered null in the examples, what means that the lining is placed immediately after the excavation of the soil mass.

Table 1 – Analysis parameters.

Parameter	Nomenclature	Unit	Value
Tunnel parameters			
Outer radius	Re	m	1
Inner radius	Ri	m	0,9
Height	H	m	20 - 16 - 10
Soil parameters			
Specific weight	γ	N/m ³	20000
Poisson ratio	ν	adm	0.3
Young modulus	E	MPa	30
Earth pressure coefficient	K	adm	0.5
Cohesion	C	MPa	0.5
Friction angle	Φ	°	30
Dilatancy angle	ψ	°	10
Lining parameters: concrete			
Poisson ratio	ν	adm	0.2
Young modulus	E	MPa	30000
Compressive strength	fck	MPa	30
Lining parameters: steel			
Poisson ratio	ν	adm	0.3
Young modulus	E	MPa	210000
Yield stress	fya	MPa	500
Reinforcement ratio	ρ	%	0.173

The analysis results, for three H / D relations (5, 8 e 10) are exhibit in the Tab. 2, 3 e 4, where the convergence, in %, is given in three points of the tunnel cross-section, for each concrete behavior model.

Table 2 - Results of the convergence (%) in the analysis with $H/D = 5$ for each concrete behavior model.

Point (°)	H/D = 5		
	Elastic	Viscoelastic	Viscoelastic w/ cracking
90	0.2701	0.3069	0.3072
180	0.0539	0.0744	0.0746
270	0.2343	0.2662	0.2663

Table 3 - Results of the convergence (%) in the analysis with $H/D = 8$ for each concrete behavior model.

Point (°)	H/D = 8		
	Elastic	Viscoelastic	Viscoelastic w/ cracking
90	0.5048	0.5637	0.5822
180	0.1314	0.1644	0.1784
270	0.4840	0.5378	0.5598

Table 4 - Results of the convergence (%) in the analysis with $H/D = 10$ for each concrete behavior model

Point (°)	H/D = 10		
	Elastic	Viscoelastic	Viscoelastic w/ cracking
90	0.6226	0.6959	0.7377
180	0.1658	0.2076	0.2414
270	0.6103	0.6782	0.7165

By analyzing the results shown in Tab. 2, 3 and 4, it can be noted that the displacements found for the tunnels with $H / D = 8$ and $H / D = 10$ grow from the elastic model to the viscoelastic one, and also increase again when considering cracking. In the example with $H / D = 5$, however, the difference only occurred from the elastic model to the viscoelastic, without considerable changes in the displacements when considering cracking. This occurs due to the lower pressure levels at which the tunnel is subjected in this smaller depth ($H = 10m$), not causing tensile stresses sufficient for the concrete to crack. In the same way, it can be seen that this difference considering cracking is greater when the tunnel is at a higher depth and subjected to higher pressures (tunnel case with $H = 20m$ compared with $H = 16m$). This consideration is important, since tunnels with larger diameters than the studied ($D = 2m$) may be located at higher depths than those analyzed and still be considered as a shallow tunnel.

The relative difference, from the elastic model to the viscoelastic model and from the viscoelastic model to the viscoelastic model with cracking, for each example of tunnel H / D relation, in the three positions analyzed, is shown in the Tab. 5.

Table 5 – Relative difference in the convergence values for each model of concrete material.

Point (°)	From elastic to viscoelastic model	From viscoelastic to viscoelastic w/ cracking model
	H/D = 5	
90	13.64%	0.08%
180	37.98%	0.37%
270	13.59%	0.05%
H/D = 8		
90	11.67%	3.27%
180	25.11%	8.48%
270	11.12%	4.09%
H/D = 10		
90	11.76%	6.01%
180	25.23%	16.27%
270	11.13%	5.65%

It is also performed a simplified parametric analysis with the aim to study the influence of some parameters in the magnitude of the final convergence when considering the cracking in the lining model. The properties of the tunnel and the materials are the same used in the previous simulations and shown in the Tab. 1, setting the height ($H = 16m$) and applying variations in the following properties: the unlined length (d_0), the characteristic compressive strength of the concrete (f_{ck}) and the Young modulus of the soil mass (E_m). The results are presented in the Fig. 6,7 and 8.

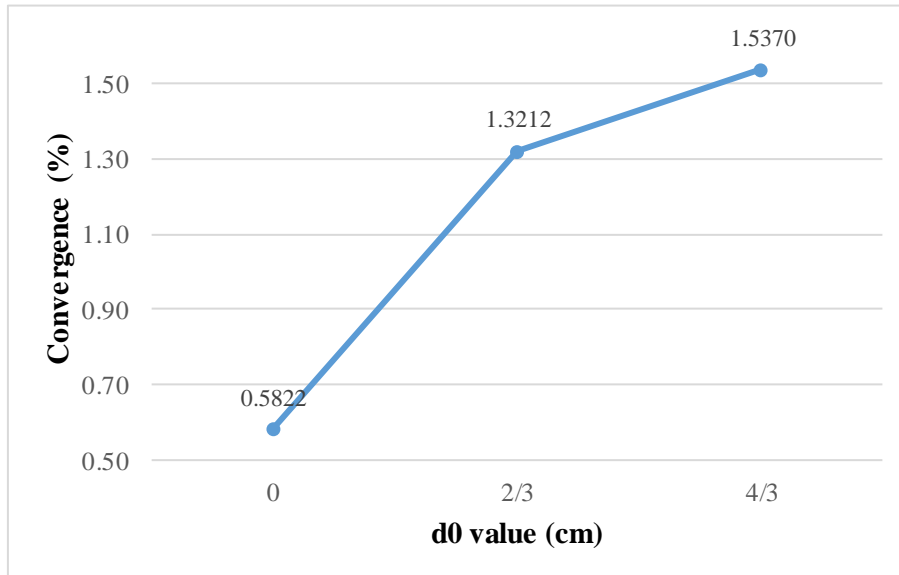


Figure 6 - Variation of the final convergence according to the unlined length (d_0).

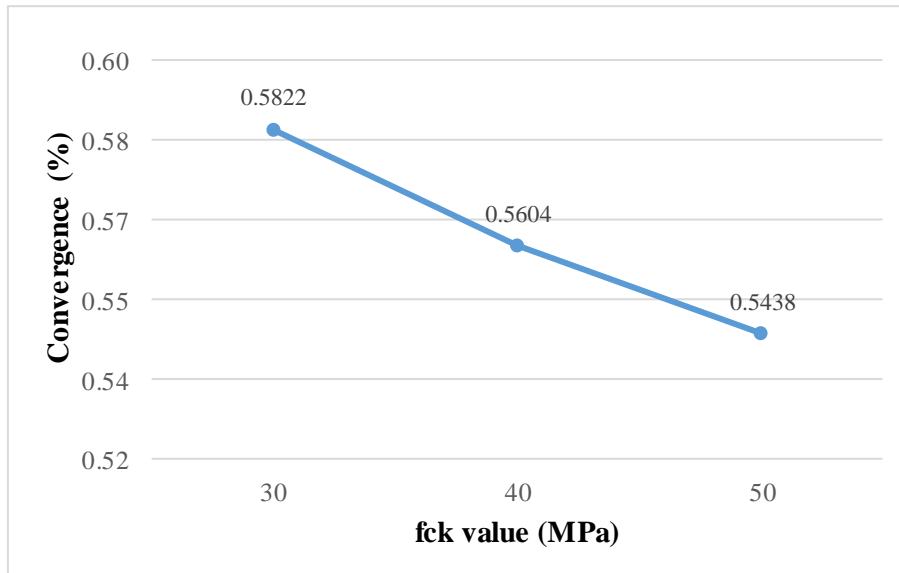


Figure 7 - Variation of the final convergence according to the compressive strength of the concrete.

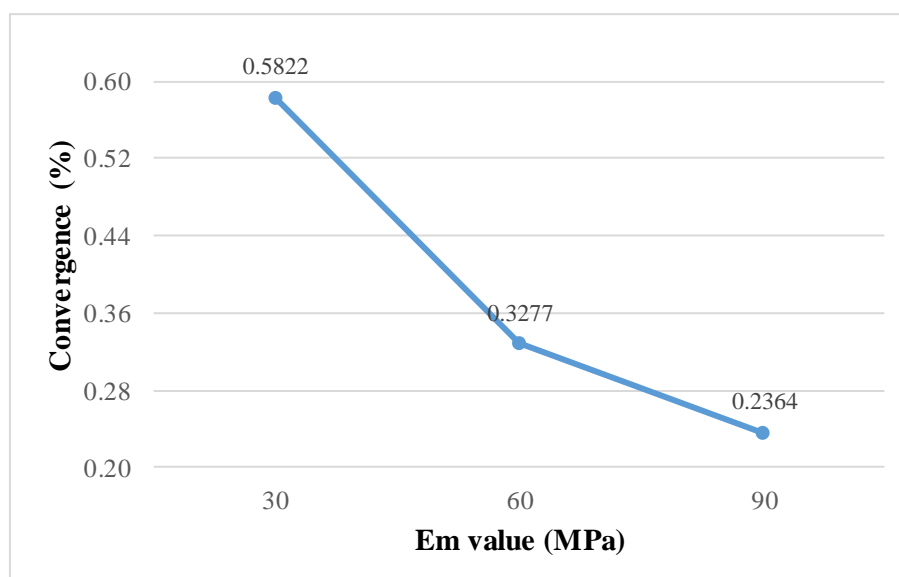


Figure 8 - Variation of the final convergence according to the Young modulus of the soil mass.

As exposed by the results shown in the figures above, the convergence is greater for larger unlined lengths, which is related to the contribution of the lining to the tunnel support: the longer it takes to place the lining, the more the tunnel deforms, considering only on the resistance of the soil mass in this initial gap. On the other hand, this greater strain of the soil mass implies smaller pressures acting on the lining, which attenuates the appearance of cracking. In addition, the convergence values decrease with both concrete and soil mass stiffness increase. This is because of the stiffer the material, the more pressures it supports and, as a result, the fewer displacements are found in the cross-section. Furthermore, cracking also influences: the smaller the f_{ck} , for example, the smaller is also the concrete tensile strength and, accordingly, more propitious this concrete to crack, causing greater displacements. However, the influence of these parameters is interactive, since the relative stiffness between the soil mass and the lining also affects the distribution of the stresses, so that the greater the stiffness of the concrete in comparison to the ground, the higher tensile stresses may arise.

5 Conclusions

From the results obtained in this study, it was possible to observe that the consideration of cracking effects in the behavior of reinforced concrete tunnel linings causes larger displacements in the tunnel cross-section than those calculated considering the concrete with elastic or viscoelastic behavior. For the example with greater depth and, therefore, submitted to larger loads, this difference reached 16.3% in one of the cross-section points, analyzing the final convergence at a point distant from the excavation front.

By setting the other parameters and changing the unlined length (d_0), the characteristic compressive strength of concrete (f_{ck}) and the Young modulus of the soil mass (E_m), convergence results were higher for larger unlined lengths and for smaller values of f_{ck} and E_m . These influences are interactive because, while they interfere directly in the magnitude of the displacements, they also interfere in the formation of cracks which, in turn, causes greater strains and, consequently, greater displacements in the concrete section.

Acknowledgements

The authors recognize and would like to thank the support of the Federal University of Rio Grande do Sul (UFRGS) as well as the scholarship provided by *Coordenação de Aperfeiçoamento de Pessoal*

de Nível Superior (CAPES), which encourage researchers to keep the good knowledge and the improvement of technology in Brazil.

References

- [1] ITA - Working Group on General Approaches to the Design of Tunnels. Guidelines for the design of tunnels. *Tunneling and underground space technology*, vol. 3, n. 3, pp. 237-249, 1988.
- [2] F. El-Nahas, F. El-Kadi, A. Ahmed. Interaction of tunnel linings and soft ground. *Tunneling and underground space technology*, vol. 7, n. 1, pp. 33-43, 1992.
- [3] F. Pinto, A. J. Whittle. Ground movements due to shallow tunnels in soft ground. I: Analytical solutions. *Journal of geotechnical and geoenvironmental engineering*, v. 140, n. 4, 2013.
- [4] B. M. Jensen. Modelagem tridimensional em elementos finitos de túneis superficiais revestidos em concreto armado. Dissertação de Mestrado, Universidade Federal do Rio Grande do Sul – UFRGS, 2019.
- [5] F. P. da M. Quevedo. Comportamento a longo prazo de túneis profundos revestidos com concreto: modelo em elementos finitos. Dissertação de Mestrado, Universidade Federal do Rio Grande do Sul – UFRGS, 2017.
- [6] R. J. Schmitz. Estrutura mista aço-concreto: análise de ponte composta por vigas de alma cheia. Dissertação de Mestrado, Universidade Federal do Rio Grande do Sul – UFRGS, 2017.
- [7] P. Lunardi. *Design and construction of tunnels: Analysis of Controlled Deformations in Rock and Soils (ADECO-RS)*. Springer Science & Business Media, 2008.
- [8] A. M. T. Gomes. Túneis urbanos sujeitos a solicitações não uniformes: O túnel do Largo do Carregal na cidade do Porto. Dissertação de Mestrado, Universidade do Porto, 1998.
- [9] E. C. Couto. Um modelo tridimensional para túneis escavados em rocha reforçada por tirantes passivos. Tese de Doutorado, Universidade Federal do Rio Grande do Sul – UFRGS, 2011.
- [10] I. Benamar. Etude des effets différés dans les tunnels profonds. Tese de Doutorado, Ecole Nationale des Ponts et Chaussées, 1996.
- [11] W. C. Ferrão. Estudo de túneis superficiais: influência na convergência e no perfil de assentamento. Dissertação de Mestrado, Universidade Federal do Rio Grande do Sul – UFRGS, 2018.
- [12] R. B. Peck. Deep excavations and tunneling in soft ground. Proc. 7th Int. Con. SMFE, State of the Art, pp. 225-290, 1969.
- [13] Ansys, Inc. Element Reference. Release 12.0, 2009.
- [14] P. M. Lazzari. Simulação numérica das etapas construtivas de pontes estaiadas através do método dos elementos finitos. Tese de Doutorado, Universidade Federal do Rio Grande do Sul - UFRGS, 2016.
- [15] F. P. M. Quevedo, R. J. Schmitz, I. B. Morsch, A. Campos Filho e D. Bernaud. Customization of a software of finite elements to analysis of concrete structures: long-term effects. *RIEM-IBRACON Structures and Materials Journal*, v. 11, n. 4, 2018.
- [16] Z. P. Bazant and S. Prasannan. Solidification theory for aging creep. *Cement and concrete research*. USA, v. 18, n. 6, pp. 923-932, 1988.
- [17] COMITÉ EURO-INTERNATIONAL DU BÉTON. CEB-FIP Model Code 1990. Thomas Telford: London, 1993.
- [18] N. S. Ottosen. A failure criterion for concrete. American Society of Civil Engineers. Engineering Mechanics Division. Journal, v. 103, n. 4, pp. 527-535, 1977.
- [19] M. Martinelli. Modelagem de situações de punção em lajes de concreto armado através do Método dos Elementos Finitos. Dissertação de mestrado, Universidade Federal do Rio Grande do Sul - UFRGS, 2003.
- [20] E. Hinton. Numerical methods and software for dynamic analysis of plates and shells. Pineridge Press, 1988.